Journal of Materials Chemistry

Dynamic Article Links

Cite this: J. Mater. Chem., 2012, 22, 11957

www.rsc.org/materials

PAPER

Rapid and facile synthesis of a $(Zn_xAg_yIn_z)S_2$ nanocrystal library *via* sono-combichem method and its characterization including single nanocrystal analysis†

Seung Jae Lee,‡[ac] Younggyu Kim,‡[b] Jongjin Jung,[a] Mi Ae Kim,[a] Namdoo Kim,[b] Seong Jin Lee,[a] Seong Keun Kim,[b] Yong-Rok Kim[c] and Joung Kyu Park*[a]

Received 24th March 2012, Accepted 26th April 2012
DOI: 10.1039/c2jm31838e

We have developed a facile and rapid synthesis of a highly fluorescent nanocrystal (NC) library, based on ultrasonic and combinatorial chemistry. Among a total of 66 tZAIS ($(Zn_xAg_yIn_z)S_2$) NCs, many NCs are highly fluorescent upon UV irradiation, and are categorized into blue, green, yellow, orange, and red by their distinct emission wavelength ranges. The tZAIS NCs not only have long fluorescence lifetimes, but also show comparable or even higher brightness than QDs without photoblinking in single NC analysis. Their unique photophysical properties together with less-toxic nature can permit the tZAIS system to be practically utilized in various bioimaging fields, especially single nanoparticle-based imaging and tracking.

Introduction

There has been remarkable achievement in the development of quantum dots (QDs), including II–VI compounds, for in the areas of sensors,[1] solar cells,[2] optical devices,[3] and imaging probes.[4–6] Especially, QDs as bioimaging probes has gained a great attention because of their excellent and unique fluorescence properties such as brightness, photostability, size dependence in emission wavelength.[7,8] The use of QDs for industrial and biological applications, however, has been limited mainly due to the serious toxicity of their heavy metal components such as cadmium, selenium, and tellurium.[9] Thus far, many research groups have reported the synthesis of less-toxic luminescent nanocrystals that do not contain such heavy metals. They include InP, InP/ZnS, $CuInS_2$, $AgInS_2$, and ZnS–$AgInS_2$ (ZAIS).[10–15] Nevertheless, multiple drawbacks such as the lack of diverse emission colors, low fluorescence intensities, and delicate synthetic parameters have impeded the progress to replace QDs. To harness the unexplored potential of less-toxic luminescent nanocrystals (NCs), it will certainly be desirable to generate a library of such NCs exhibiting various distinct emission profiles and subsequently to screen a set of proper NCs by facile and rapid high throughput format synthesis and analysis.[16–18] Our critical factors for this task include combinatorial chemistry and simple reaction conditions to control the whole process. Here, we introduce a novel strategy for the fast synthesis of high quality $(Zn_xAg_yIn_z)S_2$ nanocrystals, the modified forms of ZAIS NCs, and the production of a ZAIS NC library according to the ratio of the ingredients. The application of sonochemistry[19] together with a combinatorial chemistry allows us to assess the emission color tuning generated by a variety of different combinations among Zn, Ag, and In elements. To explore the feasibility of the ZAIS NC as a bioimaging probe, several analyses were performed including agarose gel electrophoresis, cell imaging by confocal fluorescence microscopy, and single nanoparticle imaging at 488 nm laser light, which is a routinely used excitation wavelength for bioimaging due to the reduction of damage to tissues.

ZAIS is composed of a group II alloyed with I–III–VI semiconductor nanocrystals ($ZnAgInS_2$) and their fluorescence properties can be determined simply by varying their composition without size-dependent band gap change. For a facile modulation of Zn, Ag, and In fractions to trace the effect of each component on fluorescence emission profiles, we construct the ternary forms of ZAIS (tZAIS) NCs $(Zn_xAg_yIn_z)S_2$, where $x + y + z = 1$ and their ratio can be changed within a defined total amount. Thus, the tZAIS combinatorial library was obtained by using a ternary-type composition array including 66 different combinations of three elements (see Fig. 1 and S1 in ESI†).

To establish a facile and rapid synthesis and screening procedure, we have developed and applied the sonochemical synthetic route[20] in parallel with combinatorial chemistry[21,22] that covers

[a]*Research Center for Convergence Nanotechnology, Korea Research Institute of Chemical Technology, Daejeon 305-600, Korea. E-mail: parkjk@krict.re.kr; Fax: +82-42-860-7508; Tel: +82-42-860-7373*
[b]*Department of Chemistry and WCU Department of Biophysics and Chemical Biology, Seoul National University, Seoul 151-747, Korea*
[c]*Department of Chemistry, Yonsei University, Seoul 120-747, Korea*
† Electronic supplementary information (ESI) available. See DOI: 10.1039/c2jm31838e
‡ Seung Jae Lee and Younggyu Kim contributed equally.

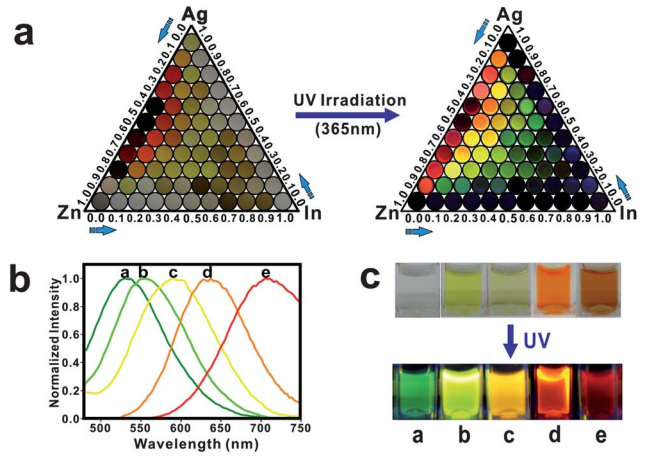

Fig. 1 Physical property of $(Zn_xAg_yIn_z)S_2$ nanocrystals (NCs). (a) A library of $(Zn_xAg_yIn_z)S_2$ NCs with 66 different combinations of composition. Their fluorescence and brightness are visualized by UV light illumination at 365 nm. (b) Emission spectra of ternary forms of ZAIS (tZAIS) NCs with different color profiles. (c) Picture of water-soluble MPA-coated $(Zn_xAg_yIn_z)S_2$ NCs ((a) $(Zn_{0.4}Ag_{0.1}In_{0.5})S_2$ [tZAIS 50], (b) $(Zn_{0.3}Ag_{0.2}In_{0.5})S_2$ [tZAIS 49], (c) $(Zn_{0.2}Ag_{0.3}In_{0.5})S_2$ [tZAIS 48], (d) $(Zn_{0.1}Ag_{0.4}In_{0.5})S_2$ [tZAIS 47], (e) $(Zn_0Ag_{0.5}In_{0.5})S_2$ [tZAIS 46]). The numbering system of each NC is shown in Fig. S1†.

a variety of different combinations in the composition of Zn, Ag, and In. Subsequently, the resulting set of NCs was analyzed by visualizing their fluorescence properties upon UV irradiation (Fig. 1a) and by measuring their emission profiles using a fluorometer (Fig. 1b). The sonochemistry utilizes ultrasound to introduce a rapid reaction time and milder operating conditions (*e.g.*, relatively lower temperature and pressure) than other temperature-based systems,[14,18,23] and eliminates cumbersome synthesis steps of other methods. The effect of ultrasonic radiation on a reaction is attributed to the acoustic cavitations within collapsing bubbles which generate localized hot spots with extreme conditions (temperature = 5000 K, pressure = 1800 atm, and cooling rate = 10^{10} K s^{-1}).[19]

Experimental section

Synthesis of precursor and $(Zn_xAg_yIn_z)S_2$ nanocrystals (NCs)

As a precursor, metal ion–diethyldithiocarbamate chelating complexes were prepared by slow drop-wise addition of 3 ml of aqueous solution including metal ions ($Zn(NO_3)_2 \cdot 6H_2O$, $AgNO_3$, $In(NO_3)_3 \cdot 3H_2O$) with various molar ratios [$(Zn_xAg_yIn_z)S_2$, $x + y + z = 1$ mole] into 30 ml of an aqueous solution containing an excess of sodium diethyldithiocarbamate for sufficient chelation between the metal ion and diethyldithiocarbamate. Resulting precursors were washed with distilled water several times and dried in an electric oven (ON-22GW, JEIO Tech, Korea). 100 mg of the precursor powder and 10 ml of dodecylamine were added into a 20 ml vial and ultrasonically treated (Sonic dismembrator Model 500, Fisher Scientific, USA) for 10 min (maximum temperature at about 160 °C) at 20 kHz power in air. The resulting suspension was centrifuged to remove by-products and washed with chloroform and methanol several times. The final products were re-dispersed in chloroform.

Synthesis of water soluble $(Zn_xAg_yIn_z)S_2$ nanocrystals (NCs)

$(Zn_xAg_yIn_z)S_2$ NCs were subjected to the ligand exchange method as mentioned in the main text. 400 μl 3-mercaptopropionic acid (MPA) was diluted in 10 ml methanol solution and subsequently 1 M KOH was added to bring the pH up over 13. The solution was combined with each $(Zn_xAg_yIn_z)S_2$ NC, and the mixture was vigorously stirred for 30 min. Then the sample was centrifuged and washed several times with methanol. The final product was re-dispersed in distilled water.

Characterization of $(Zn_xAg_yIn_z)S_2$ NCs

The resulting nanocrystals were analyzed using a Rigaku D/MAX-2200V X-ray diffractometer (Rigaku, Japan) with CuKα radiation (Ni filter). TEM and HRTEM images were obtained using a JEM-2100F field emission electron microscope (JEOL, Japan) at an accelerating voltage of 200 kV. Energy-dispersive X-ray spectroscopy (EDS) measurement was performed using Quantax 200 energy dispersive X-ray spectrometer (Bruker, Germany). Key parameters for the measurement are: (i) energy resolution was less than 127 V and peak shift (5–300 kcps) was less than 5 eV; (ii) Si Drift Detector (SDD) was utilized for data collection and the detected species were from Be ($z = 4$) to Am ($z = 95$).

Confocal imaging of single nanocrystals (ZAIS NCs and CdSe/ZnS QDs)

Confocal images of single NCs were collected using a home-built confocal laser scanning imaging system. The sample on the stage was illuminated by laser lights at both 488 nm (±5 nm) and 455 nm (±25 nm) with 12 μW powers. MaiTai (Spectra-Physics, Santa Clara, CA) femto-second pulsed laser with 80 MHz repetition rates was used as a light source. Horizontally polarized light from the laser was depolarized after it passed through the supercontinuum generation fiber (Femtowhite 800, NKT Photonics, Birkerød, Denmark), and band-pass filters were utilized to optimize the condition. Samples were illuminated on a piezo stage (NanoMax-TS, Thorlabs, Newton, NJ) coupled with an objective (Leica, 100×, 1.4 oil immersion). Emitted photons from single NCs were collected through 500 nm long-pass filter. Avalanche Photodiode (APD) was used as a detector (Perkin Elmer, SPCM-AQR-14-FC).

As a control, CdSe/ZnS QDs were purchased from QD Solution (Nanodot CS01-620, Korea). Diluted tZAIS 46, 47 and CdSe/ZnS (emission max. at 630 nm), CdSe (emission max. at 580 nm) QDs in chloroform were spotted on thin glass coverslips (Glaswarenfabrik Karl Hecht, GmbH & Co KG, 22 × 22 mm), and 15 μl of mounting medium (TDE; thiodiethanol) was added on another thin cover glass (Deckgläser, 24 × 60 mm) to match the difference of refractive indices. Subsequently, the samples were sandwiched by the cover glasses, followed by sealing with nail polish. The scanned area of the images was 4 μm × 4 μm (pixel size: 256 × 256), and dwell time per pixel was 200 μs. Using ImageJ (http://rsbweb.nih.gov/ij/, NIH, USA), image analysis and quantification of signals were performed.

Time-resolved fluorescence measurement for tZAIS 46 NCs and CdSe/ZnS QDs

Fluorescence lifetime was measured by conventional time-correlated single photon counting (TCSPC) method. TCSPC module was combined with Nanofinder 30 (Tokyo Instruments). A 40 MHz pulsed diode laser (LDH-P-C-405 with PDL 800-B driver, PICOQUANT) was used at 405 nm wavelength. The repetition rates were adjusted to 2.5 MHz according to the decay time window of each sample. The detection of single photon and determination of its arrival time in the signal period were performed using an avalanche photodiode (APD) (SPCM-AQD, Perkin Elmer, USA) and a Becker–Hickl PMS module (Becker & Hickl GmbH, Germany). tZAIS 46 NCs and CdSe/ZnS QDs were dissolved in chloroform for the measurement.

Cell culture of breast cancer cells (HCC 1954 and MCF-7) and cell viability assay

Breast cancer cell lines of MCF-7 and HCC 1954 were purchased from American Type Culture Collection (Manassas, VA) and Korean Cell Line Bank (Seoul, Korea), respectively. For confocal fluorescence imaging and cell viability assay, breast cancer cell lines were cultured according to conventional methods with slight modifications. RPMI 1954 (HCC 1954) or DMEM with high glucose (MCF-7), 10% fetal bovine serum (FBS), and Streptomycin-penicillin (Invitrogen, Carlsbad, CA) were used as growth media for these cells.

For confocal fluorescence imaging, HCC 1954 was grown in a cell culture slide with four chambers (BD Biosciences, Bedford, MA) for about one day. Each 10 μl of MPA-coated tZAIS 46 and 47 NCs (1.5 mg ml^{-1} in distilled H_2O) was added to 1 ml of RPMI 1954 media. Each 300 μl of the solution in RPMI 1954 was added into each chamber, and the sample was incubated for a day. After the ZAIS-containing media was removed, fresh RPMI 1954 media was supplied and the cells were further incubated for about 12–24 hours in RPMI 1954 media and fixed by 10% formalin solution (neutral buffered, Sigma-Aldrich). Fixed cells were washed and stored in cold Dulbecco phosphate buffered saline (DPBS) solution.

For the cell viability assay, cells were grown in 96-well plates. Cytotoxic effect was evaluated with MTT (3-[4,5-dimethylthiazol-2-yl]-2,5-diphenyltetrazolium bromide; thiazolyl blue) viability assay. MTT assay is a standard colorimetric assay that measures the activity of live-cell enzymes that reduce MTT to insoluble purple formazan crystals. Cells were seeded on 96-well plates at a density of about 1×10^4 cells per well and treated with nanocrystals at the indicated concentrations for 24 h. 1/10 volume of MTT stock (5 mg ml^{-1} in PBS) was added and further incubated for 1 h. The medium was aspirated and 100 μl of DMSO was added to each well. After 10 min of incubation, the absorbance at 570 nm was measured. All experiments were performed in triplicate.

Confocal fluorescence imaging of breast cancer cells containing ZAIS NCs

For confocal imaging of HCC 1954 cells containing ZAIS NCs, an upright type laser scanning microscope was used (LSM 5 Exciter, Zeiss, Germany). Two different wavelengths (458 nm and 488 nm) from an Ar laser were utilized to illuminate the ZAIS NCs in the fixed HCC 1954 cells. Emitted fluorescence photons were passed through a dichroic mirror and a 500 long-pass filter, and were detected. The fixed cells in a cell culture slide in four chambers were scanned under an objective with a 20× magnification after the chamber frame was removed according to manufacturer's manual. 100–200 μl PBS was added to prevent the drying of the samples. A single focal plane from the Z-stacks was selected and scanned to obtain the images showing organelles.

Results and discussion

A library of tZAIS nanocrystals was synthesized by the ultrasound decomposition of precursor powders with varying ratios of the metal fractions in solid solution. The precursor powders, metal ion–diethyldithiocarbamate chelating complexes of $(Zn_xAg_yIn_z)(S_2CN(C_2H_5)_2)_4$, were dissolved in dodecylamine and treated by ultrasound for 10 min (maximum temperature reached to about 160 °C, see Fig. S2 in ESI†), and the products were washed and retrieved by centrifugation and the final products were re-dispersed in chloroform.

The metal ratio of Ag, In, and Zn for the synthesis plays a key role in constructing the library of tZAIS for the outlook of the emission color tuning in the $(Zn_xAg_yIn_z)S_2$ NC solid solutions. Under UV irradiation at 365 nm wavelength, all the compositions of the ternary $(Zn_xAg_yIn_z)S_2$ solid solutions were directly compared according to fluorescence emission spectra as well as absorption spectra (see Fig. 1, S3 and S4 in ESI†). The initial observation of fluorescence properties of the NC library is following. As the Ag concentration increases, the emission band at 602 nm [tZAIS 64] shifts to a longer wavelength of up to 726 nm [tZAIS 46] (see Fig. 1a, S1 and S3 in ESI†). Various blue-shifted colors such as yellow and green are obtained as the Zn concentration increases. In the absence of Zn, different ratios between Ag and In produce mostly red fluorescent particles whereas there is no bright color when either of the Ag or In concentrations is zero. It should be noted that the Zn concentration plays an important role in tuning the emission color of the tZAIS NCs. Most of fluorescent compositions contain less than 50% Zn and the relative emission intensities of fluorescent tZAIS NCs from Fig. S4† are plotted as shown in Fig. S5†. We further analyzed a set of NCs because some cases might have emissions below 450 nm and the obtained emission spectra in the Fig. S4† do not cover this range. Those NCs are tZAIS 11, 15, 16, 21, 38, and 45. The emission range of the NCs shown in Fig. S6† is blue except tZAIS 11, that is ZnS (known to emit a violet color).[24] In the case of the tZAIS 21 and 38, the emission ranges cover a large region (400–600 nm) and neither spectra shows a single Gaussian curve, indicating that there are double or multiple emission ranges. The results obtained by a series of analyses show that the tZAIS NCs forming the library can be categorized into blue, green, yellow, orange, and red fluorescent NPs, indicating that the fluorescence of the NCs covers the entire visible range. In the I–III–VI NCs system, the crystal defect by anion and cation off-stoichiometry was an important factor to determine PL emission. In the $(Zn_xAg_yIn_z)S_2$ systems, various ratios of Zn, Ag, and In composition result in an intrinsic

off-stoichiometry effect which gives them the ability to induce different emission properties.[40]

Among all those fluorescent NCs, we chose two NCs, tZAIS 46 and tZAIS 47, for in-depth characterization of the tZAIS system. Transmission electron microscopy (TEM) images of tZAIS NCs clearly show their spherical shape with an average size of 3.9 nm and 4.1 nm, respectively (Fig. 2a). This suggests that changes in the composition of precursor powder do not greatly influence the size of $(Zn_xAg_yIn_z)S_2$ NCs. High-resolution TEM images show a clear lattice fringe (inset of the Fig. 2a).

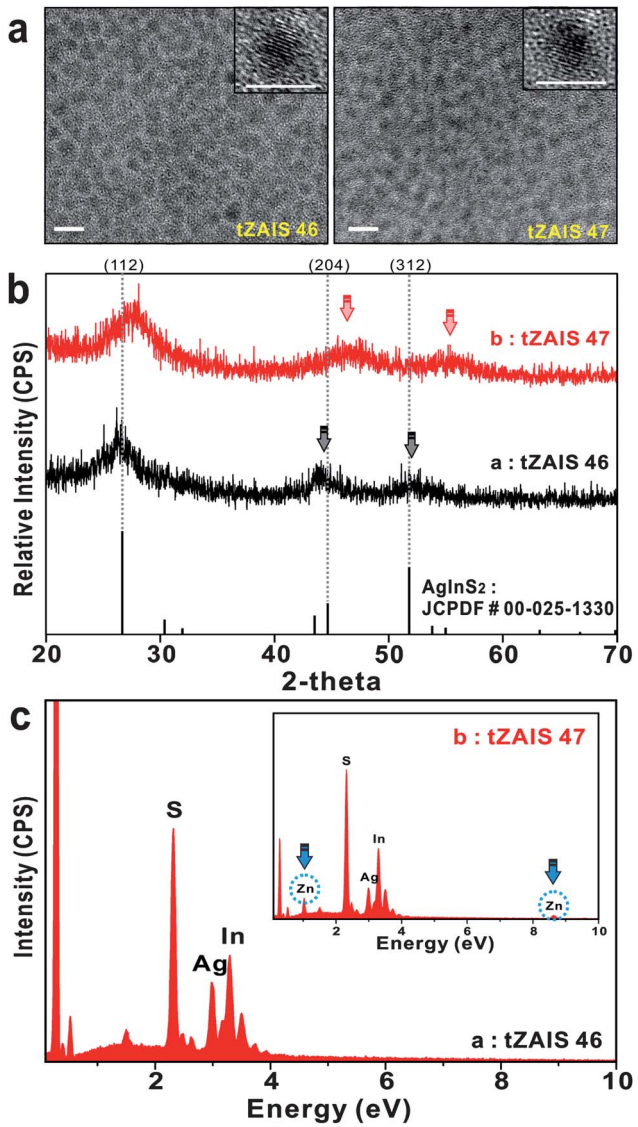

Fig. 2 Assessment of the size and composition of tZAIS NCs. (a) TEM images of $(Zn_xAg_yIn_z)S_2$ NCs for tZAIS 46 (left) and tZAIS 47 (right). Diameters of tZAIS 46 and 47 are about 3.9 nm and 4.1 nm, respectively (scale bar: 10 nm). Size distributions of both NCs are apparently homogeneous. Both tZAIS NCs show high crystallinity (inset; scale bar = 5 nm). (b) X-ray diffraction patterns of tZAIS 46 and tZAIS 47 (46: $(Zn_0Ag_{0.5}In_{0.5})S_2$, 47: $(Zn_{0.1}Ag_{0.4}In_{0.5})S_2$). CPS stands for count per second, and tZAIS 47's peaks are shifted to higher scattering angle positions due to the increase of the Zn component while tZAIS 46's peaks are exactly matched with reference peaks of $AgInS_2$. (c) Energy dispersive X-ray spectroscopy (EDS) data for tZAIS 46 and 47. The EDS data clearly show the presence of the Zn element for tZAIS 47.

The X-ray diffraction (XRD) peak positions and relative intensities of these $(Zn_xAg_yIn_z)S_2$ $(x + y + z = 1)$ solid solutions show a good agreement with crystalline tetragonal $AgInS_2$. As shown in Fig. 2b, tZAIS NCs have three broad peaks at 26.4, 44.3, and 51.9, which can be assigned to the (112), (204), and (312) planes of the tetragonal $AgInS_2$ (Joint Committee on Powder Diffraction Standards (JCPDF) # 00-025-1330), and the synthesized samples did not contain any noticeable indication of other types of structures. When the Zn ion is added to change the composition from tZAIS 46 to 47, the diffraction peak positions are shifted to higher scattering angles and the main peak moves the position of the cubic ZnS phase (JCPDF; # 01-072-4841) peak.[18] For confirmation of the presence or absence of the Zn element, we used energy dispersive X-ray spectroscopy. As shown in Fig. 2c, tZAIS 46 NCs did not show the Zn element, whereas tZAIS 47 NCs do show the Zn element (inset figure in Fig. 2c). The PL quantum yields of tZAIS 46 and 47 were measured by comparing the integrated emission of NC samples with that of Rhodamine 6G. The PL quantum yields of the tZAIS 46 and 47 were found to be 11 and 20.9%, respectively.[40]

To evaluate ZAIS NCs as a bioimaging probe, we compared the photophysical properties of tZAIS 46 NCs with commercially available CdSe/ZnS QDs (see Fig. S7 in ESI†). Single nanocrystals were imaged using a home-built confocal microscope system, and the feasibility of the NCs as bright, stable and trackable fluorophores was assessed to meet the current need in the bioimaging field.[25–27] According to our analysis, as shown in Fig. 3 and S11†, the fluorescence intensity of single tZAIS 46 NCs is higher than CdSe/ZnS QDs (emission maxima of both NCs are 630 nm) and apparently there are no typical phenomena of photoblinking, different from that of CdSe/ZnS QDs[28,29] (QDs in the blinking state are marked with white spotted circles, Fig. 3b). The fluorescence intensity-wise distribution of individual tZAIS 46 NCs and QDs at 488 nm excitation were plotted in Fig. S11† by particle-by-particle measurement. (Total intensity of each nanocrystal was calculated by multiplying area and mean intensity using ImageJ.) Distribution of the total 135 nanocrystals proves that tZAIS NCs were much brighter than CdSe/ZnS QDs at 488 nm excitation. We further evaluated the lifetime of these two NCs by time-correlated single photon counting (TCSPC).[30,31] Compared to lifetimes for CdSe/ZnS QDs (22.1 ns: 65.2%, 9.1 ns: 34.8%) as reported,[32] tZAIS 46 NCs show much longer decay times (290.5 ns: 91.1%, 9.1 ns: 8.9%) in Fig. 4. In addition, we analyzed the emitted photon trajectories from a single tZAIS NC and a CdSe/ZnS QD. tZAIS NC didn't show a dark state transition by blinking its intensity level, whereas CdSe/ZnS showed clear fluorescence intermittency from photophysical transitions between 'dark' states and 'bright' states (Fig. 5). Moreover, the amount of photons in a certain time unit (intensity) of single tZAIS 46 NC was 7–10 times higher than single CdSe/ZnS QD, which supports the analysis of the confocal images in Fig. 3. Overall, tZAIS NCs exhibit excellent properties suitable for single nanoparticle imaging, such as superior fluorescent intensity and strong stability without photoblinking. Furthermore, the longer lifetimes can be applied as a probe for fluorescence lifetime imaging[33] and characterization of detailed dynamic states.[34] Like QDs, the broad emission range is an

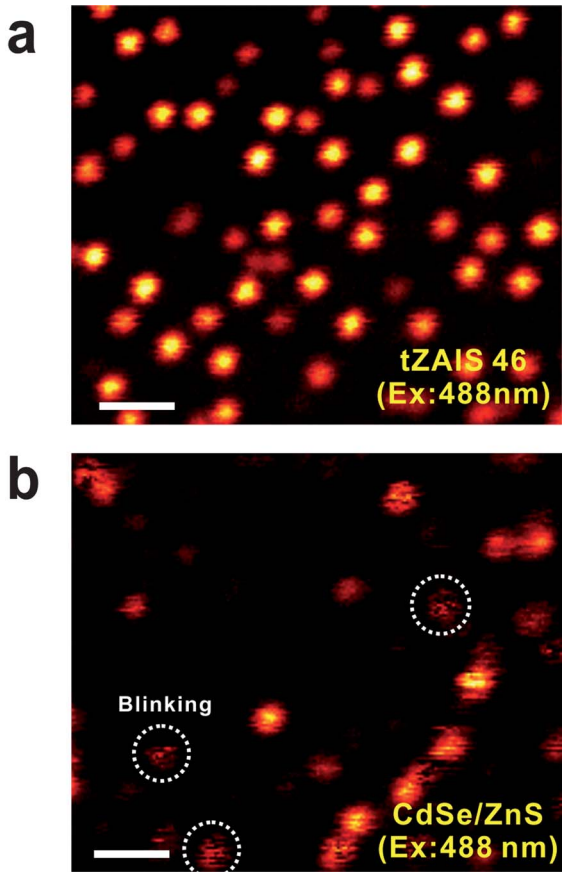

Fig. 3 Confocal images of single ZAIS nanocrystals (NC) (a) and single quantum dots (b). tZAIS 46 NCs exhibit much stronger intensity, compared to CdSe/ZnS QDs when these NCs were excited by laser light at 488 nm and emitted photons were collected through a 500 nm long-pass filter. Both ZAIS NCs and QDs have emission maxima at 630 nm. Scale bar is 500 nm.

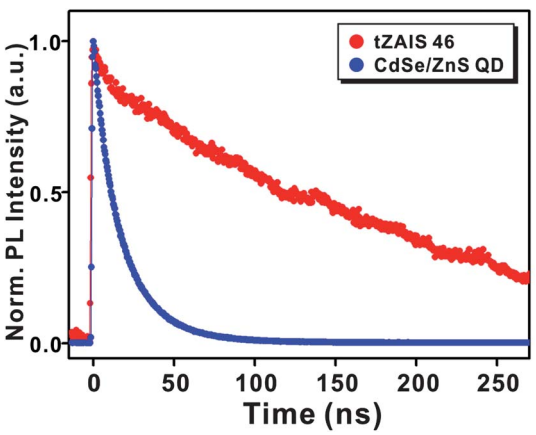

Fig. 4 Photoluminescence decay of tZAIS 46 NCs (red) and CdSe/ZnS QDs (blue). Lifetimes of tZAIS 46 NCs are 290.5 ns (91.1%) and 6.0 ns (8.9%). Lifetimes of CdSe/ZnS QDs are 22 ns (65.2%) and 9.1 ns (34.8%).

intrinsic property of solid solution-based NCs (see Fig. S7 in ESI†). Nevertheless, different NCs could be distinguished by the selection of proper band-pass filters to detect narrow emission ranges, thereby permitting multi-color imaging.[35,36]

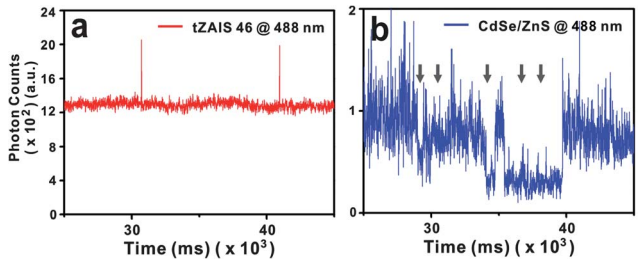

Fig. 5 Photon trajectories from a single tZAIS 46 NC (a) and CdSe/ZnS QD (b). The intensity of tZAIS 46 is 7–10 times higher than that of the QD. No photoblinking was seen from tZAIS 46 NC during 160 second acquisition time, different from CdSe/ZnS QD (gray arrows) (see Fig. S8 in ESI†).

We produced the water-soluble tZAIS nanocrystals by a ligand exchange method with 3-mercaptopropionic acid (MPA) (Fig. 6a)[37] because the water solubility is a prerequisite for biological applications. Fig. 1b and c show the photoluminescence spectra and fluorescence images of the water-soluble MPA-tZAIS NCs ((a) $(Zn_{0.4}Ag_{0.1}In_{0.5})S_2$, (b) $(Zn_{0.3}Ag_{0.2}In_{0.5})S_2$, (c) $(Zn_{0.2}Ag_{0.3}In_{0.5})S_2$, (d) $(Zn_{0.1}Ag_{0.4}In_{0.5})S_2$, (e) $(Zn_0Ag_{0.5}In_{0.5})S_2$). Once the ligand exchange is carried out, the NCs become soluble in aqueous solution. We found that although most of the NCs are soluble, the solubility appears to be influenced by the presence of Zn in the NCs. For example, the MPA-coated tZAIS 47–50 are stable for months while tZAIS 46 shows a slow decay of the solubility. Perhaps, the interaction between Zn and thiol may play an important role for the ligand exchange and stability. The resulting NCs are analyzed by agarose gel electrophoresis. The negative charge in MPA on the NCs allows them to be run in the gel and UV illumination visualizes the NCs in the gel. Fig. 6b shows that NCs from tZAIS 46 to 49 are mobile in the electric field and are visualized simply by illumination at 365 nm by a hand-held lamp.

To check the possibility of the NCs being applied to a cell-based assay system, the MPA-coated ZAIS NCs were introduced into breast cancer cells (HCC 1954) and confocal images with a single Z focal plane from Z-stack images were obtained (Fig. 7, and see Fig. S9 in ESI†). In some cases (Fig. 7a), ZAIS NPs were spread into the cytoplasm and nucleus. During the cell-fixation process, ZAIS NCs seemed to diffuse into the cytoplasm and nucleus. In the other cases (Fig. 7b), apparently the ZAIS NCs

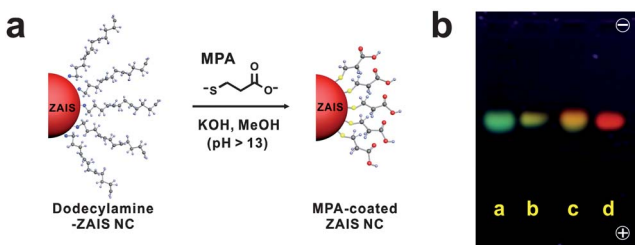

Fig. 6 (a) Preparation scheme of water-soluble tZAIS nanocrystal using 3-mercaptopropionic acid (MPA). (b) Electrophoretic analysis of water-soluble tZAIS nanocrystals on 0.8% agarose gel in Tris-borate-EDTA (TBE) buffer. Lane a, tZAIS 49; lane b, tZAIS 48; lane c, tZAIS 47; lane d, tZAIS 46.

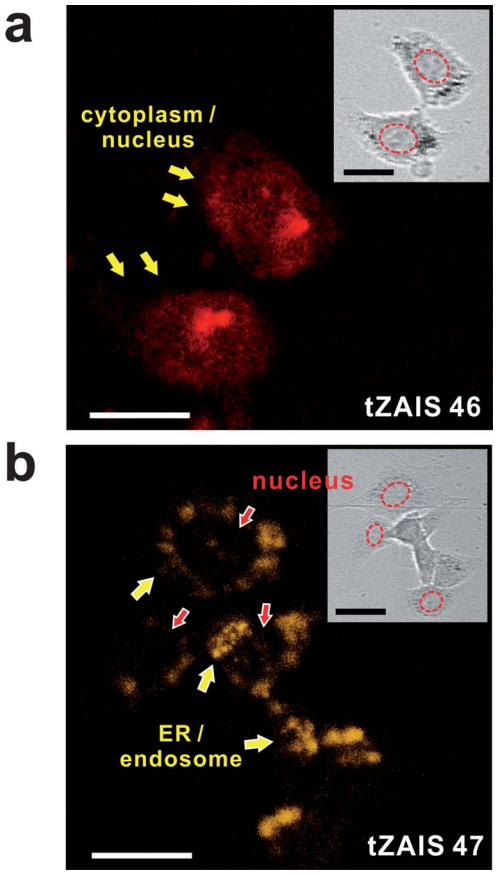

Fig. 7 Confocal images of breast cancer cells (HCC1954) containing tZAIS 46 (a) and tZAIS 47 (b). Internalized NCs in cells spread out in the cytoplasm (a) or were confined in endosomes or ER (b). The insets show bright field images of the cells. The red-dotted circles denote nucleus. Scale bar is 50 μm.

were trapped in vesicles such as endosomes, and located in the endoplasmic reticulum (ER) or Golgi organelles, indicating that the tZAIS NCs can be utilized as cell imaging fluorophores to clearly visualize detailed cellular organelles in a specific image plane of confocal microscope.

Fluorophores for biological applications have to meet multiple requirements such as excellent photophysical properties, a facile functionalization scheme for biomolecule attachment and biocompatibility without having any severe toxicity. The tZAIS NCs are photophysically suitable for *in vitro* assay and cell imaging, and can be applicable even to imaging in small animals.[35,38] Nevertheless, an additional concern regarding toxicity needs to be addressed. Thus, we evaluated the dose-dependent cytotoxicity of the $(Zn_xAg_yIn_z)S_2$ NCs at a series of different concentrations of the NCs. To assess the cytotoxic effect of the water-soluble $(Zn_xAg_yIn_z)S_2$ NCs, we tested various concentrations (two-fold serial dilutions starting from 200 g ml^{-1} of tZAIS) of each sample for a cell viability 3-[4,5-dimethylthiazol-2-yl]-2,5-diphenyltetra zolium bromide (MTT) assay.[39] The result shows that the toxicity of each of the $(Zn_xAg_yIn_z)S_2$ NCs (tZAIS 46 and 47) was not found on two cell types (HCC 1954 and MCF-7) treated with the NCs after 24 hour post addition (see Fig. 8 and S10 in ESI†).

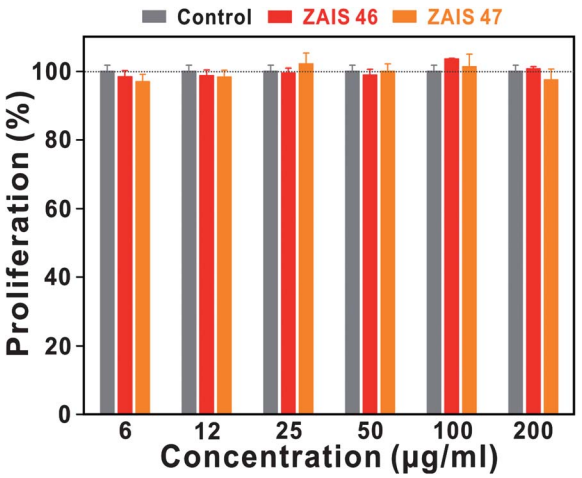

Fig. 8 MTT cell viability assay was performed to check the cell viability and cytotoxicity of tZAIS nanocrystals. There is no cytotoxic effect up to 200 μg ml^{-1} concentrations. All data are presented as mean SD.

Conclusion

In conclusion, we have successfully constructed a library of $(Zn_xAg_yIn_z)S_2$ nanocrystals containing less-toxic elements (Zn, Ag, and In) by the sono-combichem method. The ultrasound-based ZAIS nanocrystal synthesis can be utilized as a novel, simple and rapid method for creating a library of $(Zn_xAg_yIn_z)S_2$ NCs. The emission colors of the resulting NCs are tunable from blue to red, depending on their chemical composition. According to our characterization, the tZAIS NCs seem much brighter than QDs by up to about 10 times and more photostable due to their lack of photoblinking. Perhaps those are the most important features of these NCs because they allow for more reliable fluorescence studies including single particle tracking. Their compact sizes of about 4 nm, regardless of the emission colors, can also be an added value as fluorescence probes. Moreover, tZAIS NCs are non-toxic to cells as evidenced using two cell types, HCC-1954 and MCF-7, thereby showing a feasibility of their use for bioimaging. In addition, the library of $(Zn_xAg_yIn_z)S_2$ NCs could assist in photocatalysts, quantum dot-like solar cells applications and other relevant areas.

Acknowledgements

We thank Dr Jeong-O Lee and Mr Dong-Won Park at KRICT for helping us with a confocal microscope for cell imaging. We would like to gratefully acknowledge an important experimental help from Mr Ilseung Yang, Sun Jin Hwang, Hyung Jun Kim, Soon Kyu Lim, and Ms, Jung Eun Lee at Seoul National University. This research was supported by KRICT general research fund (SI-1210) and the Korean Ministry of Science and Technology (KK-1207-B6) and the Pioneer Research Center Program of the NRF (2012-0002131). Prof. S. K. K acknowledges the National Research Foundation of Korea (NRF) grant (R31-2009-100320). Prof. Y.-R. Kim thanks a grant from the National Research Foundation of Korea Grant funded by the Korean Government (no. 2011-0027695).

References

1 C. J. Murphy, *Anal. Chem.*, 2002, **74**, 520A.
2 P. V. Kamat, *J. Phys. Chem. C*, 2008, **112**, 18737.
3 P. Bhattacharya, S. Ghosh and A. D. Stiff-Roberts, *Annu. Rev. Mater. Res.*, 2004, **34**, 1.
4 V. I. Klimov, A. A. Mikhailovsky, S. Xu, A. Malko, J. A. Hollingsworth, C. A. Leatherdale, H. Eisler and M. G. Bawendi, *Science*, 2000, **290**, 314.
5 M. Bruchez, Jr, M. Moronne, P. Gin, S. Weiss and A. P. Alivisatos, *Science*, 1998, **281**, 2013.
6 P. K. Bae, K. N. Kim, S. J. Lee, H. J. Chang, C. K. Lee and J. K. Park, *Biomaterials*, 2009, **30**, 836.
7 X. Michalet, F. F. Pinaud, L. A. Bentolila, J. M. Tsay, S. Doose, J. J. Li, G. Sundaresan, A. M. Wu, S. S. Gambhir and S. Weiss, *Science*, 2005, **307**, 538.
8 I. L. Medintz, H. T. Uyeda, E. R. Goldman and H. Mattoussi, *Nat. Mater.*, 2005, **4**, 435.
9 R. Hardman, *Environ. Health Perspect.*, 2006, **114**, 165.
10 L. Li and P. Reiss, *J. Am. Chem. Soc.*, 2008, **130**, 11588.
11 S. Xu, S. Kumar and T. Nann, *J. Am. Chem. Soc.*, 2006, **128**, 1054.
12 J. Park and S.-W. Kim, *J. Mater. Chem.*, 2011, **21**, 3745.
13 X. Wang, D. Pan, D. Weng, C.-Y. Low, L. Rice, J. Han and Y. Lu, *J. Phys. Chem. C*, 2010, **114**, 17293.
14 H. Zhong, Y. Zhou, M. Ye, Y. He, J. Ye, C. He, C. Yang and Y. Li, *Chem. Mater.*, 2008, **20**, 6434.
15 Y. Hamanaka, T. Ogawa, M. Tsuzuki and T. Kuzuya, *J. Phys. Chem. C*, 2011, **115**, 1786.
16 T. Torimoto, S. Ogawa, T. Adachi, T. Kameyama, K.-I. Okazaki, T. Shibayama, A. Kudo and S. Kuwabata, *Chem. Commun.*, 2010, **46**, 2082.
17 T. Uematsu, S. Taniguchi, T. Torimoto and S. Kuwabata, *Chem. Commun.*, 2009, 7485.
18 T. Torimoto, T. Adachi, K.-i. Okazaki, M. Sakuraoka, T. Shibayama, B. Ohtani, A. Kudo and S. Kuwabata, *J. Am. Chem. Soc.*, 2007, **129**, 12388.
19 K. S. Suslick, *Science*, 1990, **247**, 1439.
20 S. J. Lee, K. N. Kim, P. K. Bae, H. J. Chang, Y.-R. Kim and J. K. Park, *Chem. Commun.*, 2008, 5574.
21 L. Tian and J. J. Vittal, *New J. Chem.*, 2007, **31**, 2083.
22 G. Liu, C. Liu and A. J. Bard, *J. Phys. Chem. C*, 2010, **114**, 20997.
23 J. J. Nairn, P. J. Shapiro, B. Twamley, T. Pounds, R. von Wandruszka, T. R. Fletcher, M. Williams, C. Wang and M. G. Norton, *Nano Lett.*, 2006, **6**, 1218.
24 H. Song, Y.-M. Leem, B.-G. Kim and Y.-T. Yu, *J. Phys. Chem. Solids*, 2008, **69**, 153.
25 T. Pons and H. Mattoussi, *Ann. Biomed. Eng.*, 2009, **37**, 1934.
26 N. Ruthardt, D. C. Lamb and C. Brauchle, *Mol. Ther.*, 2011, **19**, 1199.
27 P. Pierobon and G. Cappello, *Adv. Drug Delivery Rev.*, 2011.
28 B. Mahler, P. Spinicelli, S. Buil, X. Quelin, J. P. Hermier and B. Dubertret, *Nat. Mater.*, 2008, **7**, 659.
29 X. Wang, X. Ren, K. Kahen, M. A. Hahn, M. Rajeswaran, S. Maccagnano-Zacher, J. Silcox, G. E. Cragg, A. L. Efros and T. D. Krauss, *Nature*, 2009, **459**, 686.
30 M. Kuno, D. P. Fromm, H. F. Hamann, A. Gallagher and D. J. Nesbitt, *J. Chem. Phys.*, 2001, **115**, 1028.
31 W. Becker, H. Hickl, C. Zander, K. H. Drexhage, M. Sauer, S. Siebert and J. Wolfrum, *Rev. Sci. Instrum.*, 1999, **70**, 1835.
32 B. R. Fisher, H.-J. Eisler, N. E. Stott and M. G. Bawendi, *J. Phys. Chem. B*, 2003, **108**, 143.
33 C. W. Chang, D. Sud and M. A. Mycek, in *Methods in Cell Biology*, ed. S. Greenfield and E. W. David, Academic Press, 2007, vol. 81, pp. 495–524.
34 D. S. Talaga, *J. Phys. Chem. A*, 2009, **113**, 5251.
35 N. Kosaka, M. Ogawa, N. Sato, P. L. Choyke and H. Kobayashi, *J. Invest. Dermatol.*, 2009, **129**, 2818.
36 M. Han, X. Gao, J. Z. Su and S. Nie, *Nat. Biotechnol.*, 2001, **19**, 631.
37 B.-K. Pong, B. L. Trout and J.-Y. Lee, *Langmuir*, 2008, **24**, 5270.
38 X. Gao, Y. Cui, R. M. Levenson, L. W. Chung and S. Nie, *Nat. Biotechnol.*, 2004, **22**, 969.
39 J. Jung, A. Solanki, K. A. Memoli, K.-i. Kamei, H. Kim, M. A. Drahl, L. J. Williams, H.-R. Tseng and K. Lee, *Angew. Chem., Int. Ed.*, 2010, **49**, 103.
40 B. Chen, H. Zhong, W. Zhang, Z. Tan, Y. Li, C. Yu, T. Zhai, Y. Bando and B. Zou, *Adv. Funct. Mater.*, 2012, **22**, 2081.